ACS OMEGA

http://pubs.acs.org/journal/acsodf

Article

Facile Synthesis of Gold Nanoparticles for Anticancer, Antioxidant Applications, and Photocatalytic Degradation of Toxic Organic Pollutants

Mohamed Hosny,* Abdelazeem S. Eltaweil,* Mohamed Mostafa, Yaser A. El-Badry, Enas E. Hussein, Ahmed M. Omer, and Manal Fawzy

Cite This: *ACS Omega* 2022, 7, 3121−3133

Read Online

ACCESS | Metrics & More | Article Recommendations

ABSTRACT: In the current study, a facile, rapid, and ecologically safe photosynthesis of gold nanoparticles (AuNPs) that remained stable for 3 months is reported to advocate the main aspects of green chemistry, such as safer solvents and auxiliaries, and the use of renewable feedstock. *Zi*-AuNPs were phytosynthesized by the aqueous extract of *Ziziphus spina-christi* leaves, and numerous techniques were employed for their characterization. The results demonstrated the successful phytofabrication of crystalline AuNPs with brownish-black color, spherical nanoparticles with a size between 0 and 10 nm, a plasmon peak at 540 nm, and a surface charge of −25.7 mV. *Zi*-AuNPs showed an effective photodegradation efficiency (81.14%) against malachite green and a good recycling capacity of 69.2% after five cycles of regeneration. The cytotoxicity test by the 3-(4,5-dimethylthiazol-2-yl)-2,5-diphenyltetrazolium bromide (MTT) assay signified a high anticancer efficiency for both *Zi*-AuNPs and *Z. spina-christi* extract against human breast cancer cells (MCF7 cell line) with IC_{50}'s of 48 and 40.25 μg/mL, respectively. Highly efficient antioxidant capabilities were proven with 2,2-diphenyl-1-picrylhydrazyl (DPPH) removal percentages of 67.5% for *Zi*-AuNPs and 92.34% for *Z. spina-christi* extract.

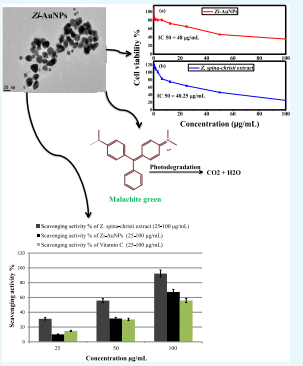

1. INTRODUCTION

Nanotechnology has been postulated as a research area that combines the principles of biology, physics, and chemistry to synthesize new materials with unique properties at a very small scale, which is the nanoscale (0−100 nm).[1,2] It is an interdisciplinary research area that involves developing, controlling, and utilizing these nanomaterials at the molecular level and in a lot of different applications.[3,4] Optoelectronic devices, catalysis, cancer treatment, drug delivery, energy, space industry, and wastewater treatment are just some examples of the applications that nanotechnology is transforming through harnessing nanomaterials owing to their extremely small particle size and high surface area that render them unique characteristics.[5,6]

Various techniques could be employed in the fabrication of nanomaterials such as chemical reduction, electrochemical synthesis, physical synthesis, and lithography. These techniques are usually expensive and hazardous because they frequently involve the use of noxious reducing agents and harsh reaction conditions.[7] On the other hand, biosynthesis of nanostructures *via* plants and microorganisms aroused as a safe, inexpensive, and more sustainable alternative.[8] Relying on microorganisms requires cautious handling and maintenance in culturing and growing of these organisms, which to some extent adds to the expenses.[9] Therefore, relying on plant extracts in the synthesis of nanomaterials has garnered most of the workers' interests owing to the existence of various phytoactive constituents in plant extracts that are working as reducing and stabilizing agents at the same time, resulting in lower cost, facile, rapid, and efficient synthesis.[10] Extracts of numerous plant species were utilized for nanomaterials production including *Potamogeton pectinatus*, *Scutellaria barbata*, and *Phragmites australis* to obtain different sized and shaped nanomaterials that could be harnessed in many applications.

Owing to their special properties such as quick synthesis, catalytic and size-dependent properties, and low toxicity, gold nanoparticles (AuNPs) are attracting more attention today in numerous applications.[11,12] AuNPs could be employed in imaging, drug delivery, and photocatalysis.[13] Production of AuNPs with different morphologies and characteristics could be accomplished through variation in the preparation conditions including pH and other factors.[5]

Received: November 28, 2021
Accepted: December 31, 2021
Published: January 11, 2022

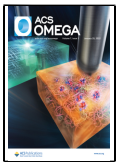

Scheme 1. Biosynthesis Procedures of *Zi*-AuNPs Colloidal Solution

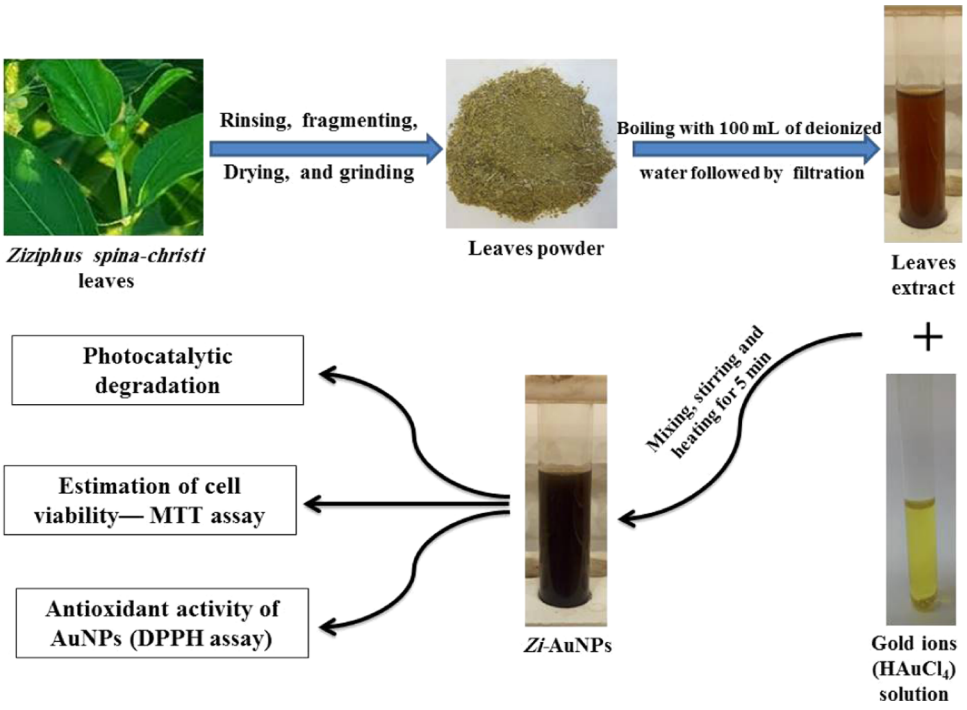

AuNPs and other nanomaterials have been widely employed in wastewater treatment to remove different types of pollutants as a result of their outstanding characteristics such as low cost and recyclability.[14,15] These pollutants have seriously threatened human health and water quality.[16] One of these toxic pollutants is malachite green (MG) dye, which is used in food coloring as well as in cloths, cotton, and wool industries.[17]

Currently, there is a high death rate from cancer in different countries and the treatment protocols are not very efficient.[18] Despite imposing deleterious impacts on human health, conventional cancer treatments are also highly expensive.[19] On this basis, there is an urgent requirement for less costly and safer methods of improving anticancer drugs and therapies.[20] Consequently, the synthesis of sustainable and low-cost anticancer agents like AuNPs was targeted in the current study.

The role of free radicals' scavengers, which are commonly known as antioxidants, was confirmed to be quintessential because of the detrimental impacts of these radicals.[21] Free radicals such as 2,2-diphenyl-1-picrylhydrazyl (DPPH) are usually removed by antioxidants.[22]

Ziziphus spina-christi is a deciduous tree that is commonly found in warm temperate and subtropical regions including the Middle East.[23] Its antimicrobial, antifungal, antioxidant, and antidiabetic potentials were meticulously investigated, and they were accredited to its phytoconstituents including flavonoids, saponins, alkaloids, glycosides, and terpenoids.[24] Therefore, the aqueous extract of *Z. spina-christi* was used in this work to phytofabricate AuNPs (*Zi*-AuNPs). Thus, the novel part of the current work is the rapid phytosynthesis of AuNPs using *Z. spina-christi* extract that were stable for about 3 months and further investigate the photocatalytic, anticancer, and antioxidant potentialities of these nanoparticles.

2. RESULTS AND DISCUSSION

Z. spina-christi was proved to possess antinociceptive, antidiabetic, antioxidant, and antibacterial properties.[24] The examination of the chemical composition of *Z. spina-christi* unraveled the existence of numerous phytoactive constituents such as alkaloids, flavonoids, glycosides, terpenoids, and tannins.[25,26] The biosynthesis procedures are provided in Scheme 1. In addition, Figure 1 displays a facile probable mechanism for the phytofabrication of *Zi*-AuNPs *via* hyperin, which is a common flavonoid in *Z. spina-christi* leaves. Hyperin and other phytoconstituents such as rutin, quercetin, isovitexin, lucoside-7-*O*-rhamnoside, and apigenin in *Z. spina-christi* aqueous extract[24] are reducing gold ions (Au^{3+}) into nano gold (Au^0). Furthermore, they contribute to the stabilization of *Zi*-AuNPs by capping them, with other phytoactive components, leading to the formation of stable *Zi*-AuNPs.

2.1. UV−Visible Analysis. In the current study, a transformation in the color from light brown to brownish-black after adding gold ions to the extract of *Z. spina-christi* and a surface plasmon resonance (SPR) peak at 540 nm denoted the successful formation of *Zi*-AuNPs (Figure 2a). The obtained results were concomitant with others stated in previous works that aimed at the phytofabrication of AuNPs using other extracts such as Sunderam et al.[27] who synthesized AuNPs using *Anacardium occidentale* leaf extract and reported a wavelength of 540 nm as well as Chen et al.[28] who observed an SPR peak at 539 nm when synthesizing AuNPs by the extract of *Curcumae kwangsiensis* leaves due to the disappearance of d−d transitions of gold ions, indicating the successful green synthesis process. Additionally, it should be stated that the synthesized *Zi*-AuNPs were stabilized for almost 3 months as presented in Figure 2b,c, demonstrating the high efficacy of *Z. spina-christi* extract in the biosynthesis of AuNPs and also its promising application in the preparation of other nanomaterials.

2.2. Fourier Transform Infrared (FT-IR) Analysis. FT-IR spectroscopy is often employed in the detection of functional groups, which are likely participating in the reduction and stabilization of phytosynthesized nanomaterials. Several bands

https://doi.org/10.1021/acsomega.1c06714
ACS Omega 2022, 7, 3121−3133

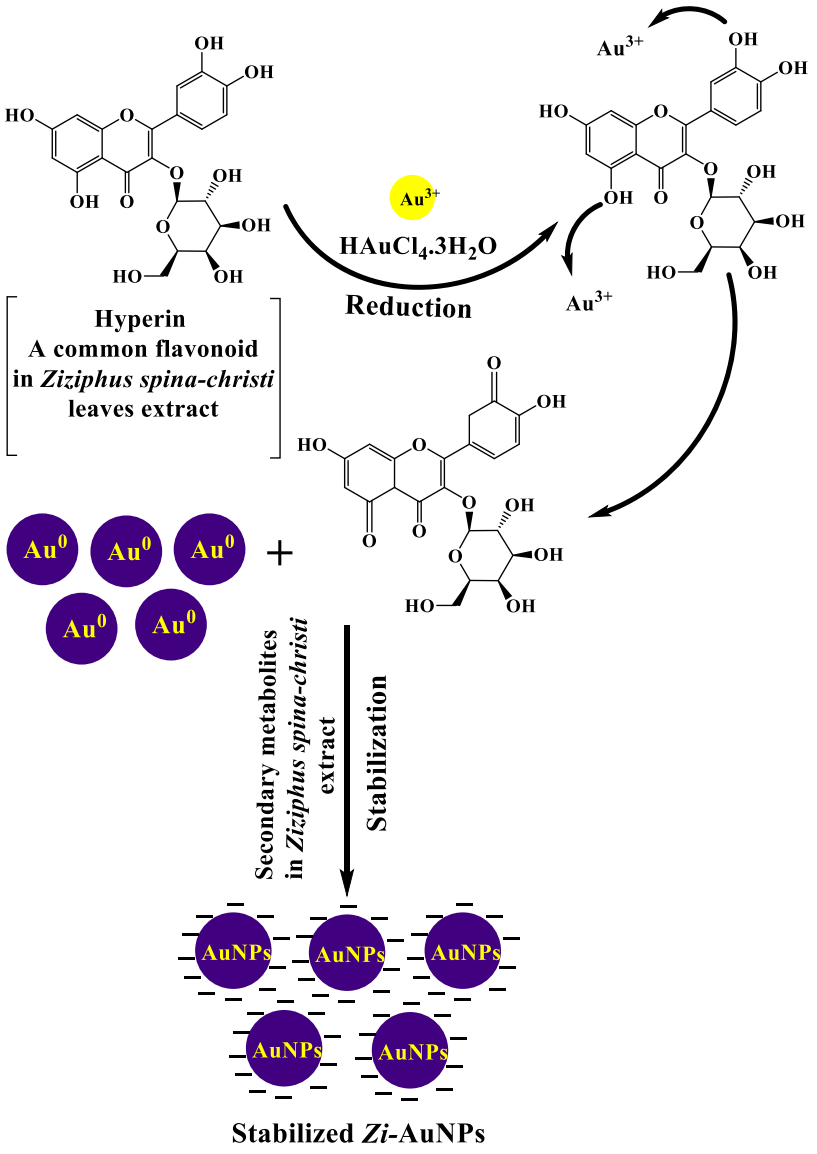

Figure 1. Proposed mechanism of *Zi*-AuNPs synthesis.

appeared in the IR spectrum of *Z. spina-christi* extract (Figure 3a) that are characteristic for different functional groups including the H-bonded O−H band at 3242 cm^{-1} that shifted to 3260 cm^{-1} in *Zi*-AuNPs accompanied with a dramatically lower intensity as shown in Figure 3b. A C−H stretch was observed at 2920 cm^{-1}, which shifted to doublet C−H at 2915 and 2845 cm^{-1}. Moreover, C═C band and C−H bending were identified at 1597 and 1400 cm^{-1}, respectively. Subsequently, they completely disappeared in the spectrum of *Zi*-AuNPs. C−O stretching appeared at 1011 cm^{-1}, which then slightly shifted to a lower wavenumber of 1002 cm^{-1} in *Zi*-AuNPs. Similar results to the current one were reported in other recent works.[29,30] Therefore, it was concluded that various phytoconstituents, especially those containing O−H functional groups, such as alkaloids, flavonoids, and tannins, were responsible for the reduction and stabilization of *Zi*-AuNPs.

2.3. High-Resolution Transmission Electron Microscopy (HRTEM) Analysis. Size, shape, and other morphological characteristics of nanoparticles could be provided by microscopy techniques. Data collected from HRTEM analysis indicated that the size of *Zi*-AuNPs ranged from less than 2 nm to more than 10 nm and the principal shape formed was spherical as shown in Figure 4a−c. Furthermore, a histogram demonstrating the various sizes of *Zi*-AuNPs is displayed in Figure 4d, indicating that the average size is 6−8 nm with around 25%. The detected particle size in this study was concluded to be smaller than that observed in many studies such as AuNPs phytosynthesized by the *Convolvulus fruticosus* extract that was around 30 nm.[31] Moreover, other shapes were observed, including rod, triangle, and others, and it was concluded that diverse shapes of phytosynthesized AuNPs are mainly formed through the various phytocomponents present in the plant extracts that have different reducing capacities.[32] Crystalline *Zi*-AuNPs had an interplanar spacing of d = 0.22 nm, which is presented in Figure 4c (inset).

2.4. X-ray Diffraction (XRD) Analysis. The face-centered cubic (FCC) crystalline structure of *Zi*-AuNPs was confirmed *via* XRD analysis that is displayed in Figure 5a as this analysis is reckoned as an essential step in determining the crystal structure of nanomaterials.[33,34] Four distinguishing peaks of Au were observed at 37.31, 44.31, 64.51, and 78.73° matching the

https://doi.org/10.1021/acsomega.1c06714
ACS Omega 2022, 7, 3121−3133

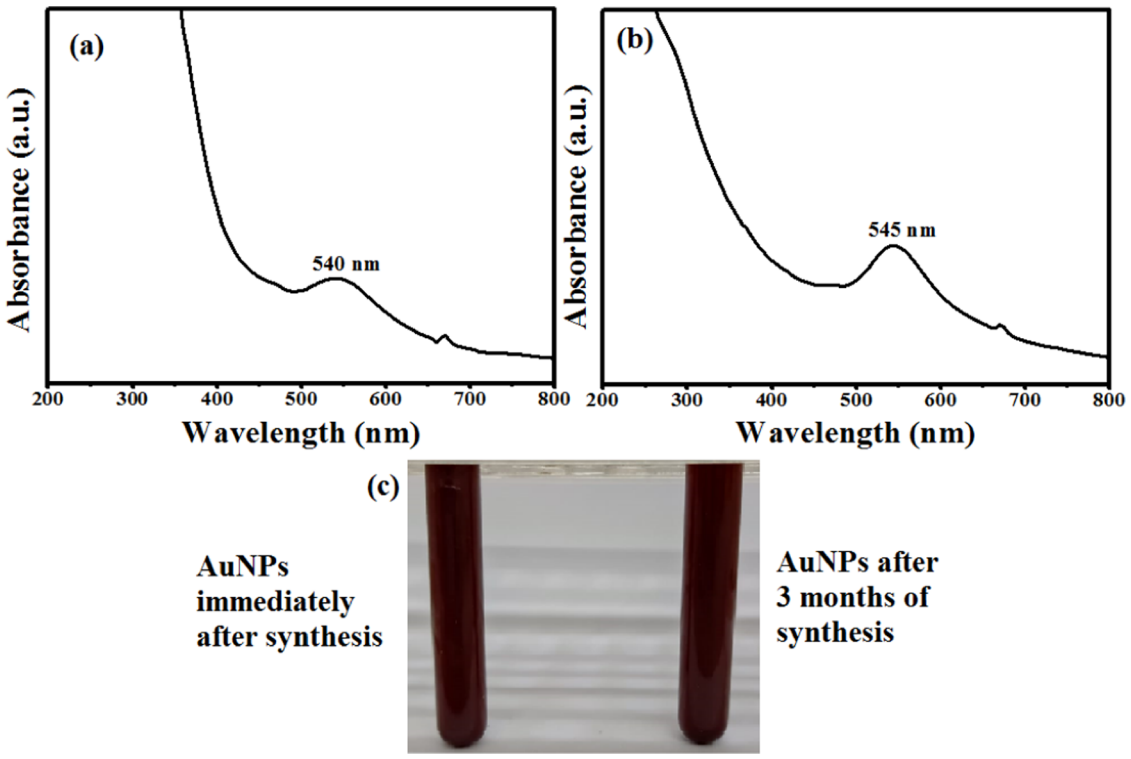

Figure 2. (a) UV−visible spectrum of immediately synthesized *Zi*-AuNPs. (b) UV−visible spectrum of *Zi*-AuNPs after 3 months. (c) Image of *Zi*-AuNPs promptly after synthesis and after 3 months.

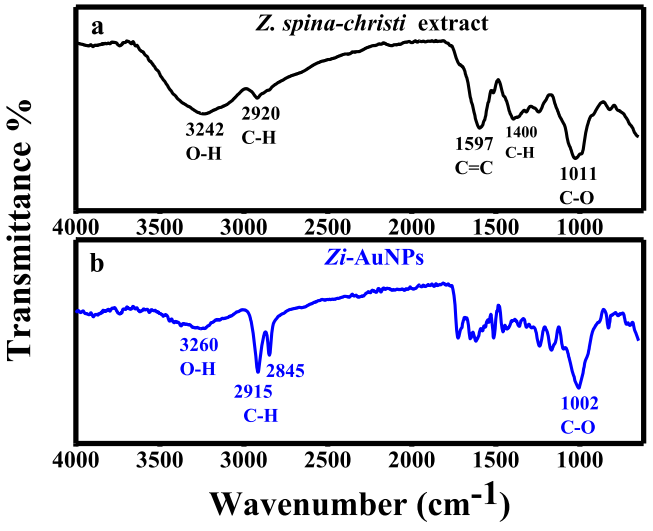

Figure 3. FT-IR spectra of (a) *Z. spina-christi* extract and (b) *Zi*-AuNPs.

planes of (111), (200), (220), and (311), respectively. Moreover, the main growth orientation was the (111) plane as previously reported in different works.[35] These values were matching the reported standards JCPDS file no. 04-0784 for crystalline Au. The crystallite size of *Zi*-AuNPs was measured by the Scherrer equation and found to be nearly 4.18 nm that was within the size range (0−10 nm) measured by HRTEM. This crystallite size was similar to that reported in another study that targeted the formation of AuNPs *via* the extract of *Atriplex halimus*,[36] which was 6.31 nm.

2.5. EDX Analysis. In the current research, the bioreduction of Au^{3+} into *Zi*-AuNPs was ensured by EDX analysis that was designated by the strong peaks of Au^0 at 2.3, 1.8, 8.5, 9.7, 11.5, and 13.4 keV as displayed in Figure 5b. These signals were concomitant with other previously reported results.[37] Signals for carbon and oxygen were observed that are deemed to be resulting from the plant extract. The production yield of *Zi*-AuNPs was found to be 20.75%, as demonstrated in Figure 5b (inset), indicating the high efficiency of the *Z. spina-christi* extract in reducing Au^{3+} into *Zi*-AuNPs.

2.6. ζ Measurement. The existence of negative charge on the *Zi*-AuNPs surface is commonly attributed to the presence of several biological constituents in *Z. spina-christi* extract that preserves the colloidal stability of *Zi*-AuNPs. The ζ-potential of *Zi*-AuNPs was −25.7 mV, as displayed in Figure 5c, at a pH value around 6 denoting the prominent role of the phytoconstituents found in *Z. spina-christi* leaf aqueous extract in preserving the stability of the phytofabricated *Zi*-AuNPs. When the obtained results were compared to previously published ones such as ref 29, it was concluded that the current ζ-potential value is better as they detected a ζ value of −7.47 mV. Thus, the high degree of stability of *Zi*-AuNPs was confirmed.

2.7. Photocatalytic Degradation. In the current study, the photodegradation of MG, which is a toxic organic pollutant usually resulting from various manmade sources *via* *Zi*-AuNPs, was examined using UV light irradiation. Two concentrations of MG were tested in the current work: 25 and 50 ppm. Regarding the lower concentration, its degradation percentage was about 81.14% after 100 min under UV irradiation, as displayed in Figure 6a. However, the photodegradation efficiency in the case of the higher concentration (Figure 6b) was 63.29% during the same time under pH 6 and 25 °C temperature and without the addition of free radicals.

When the pH of the solution was first examined within 100 min of photodegradation of MG with a concentration of 25

https://doi.org/10.1021/acsomega.1c06714
ACS Omega 2022, 7, 3121−3133

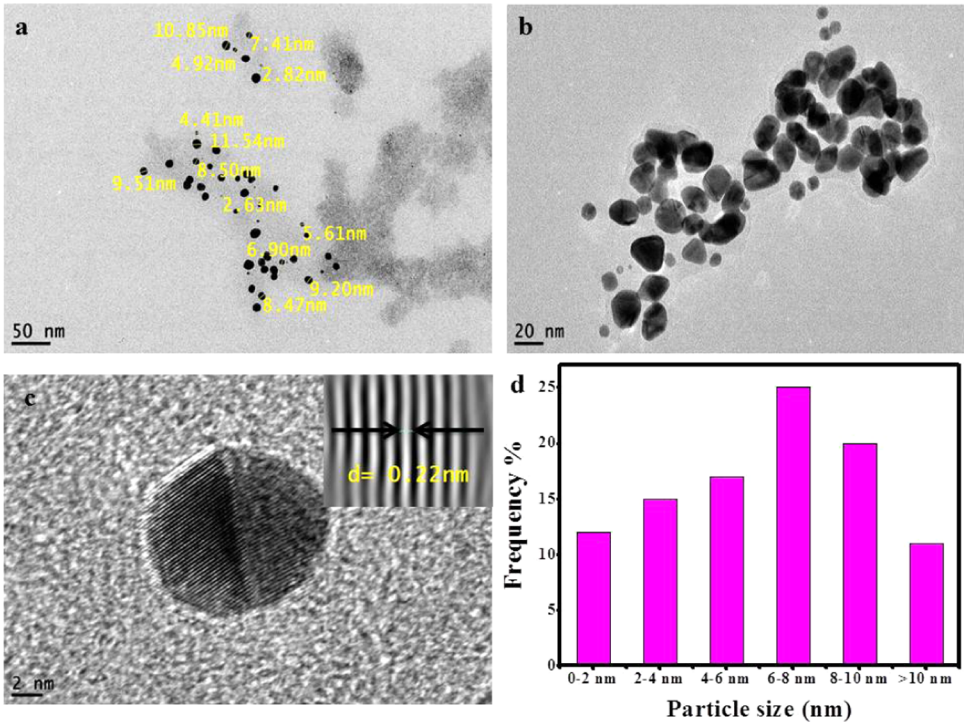

Figure 4. (a–c) HRTEM images of *Zi*-AuNPs and (d) particle size distribution histogram of *Zi*-AuNPs.

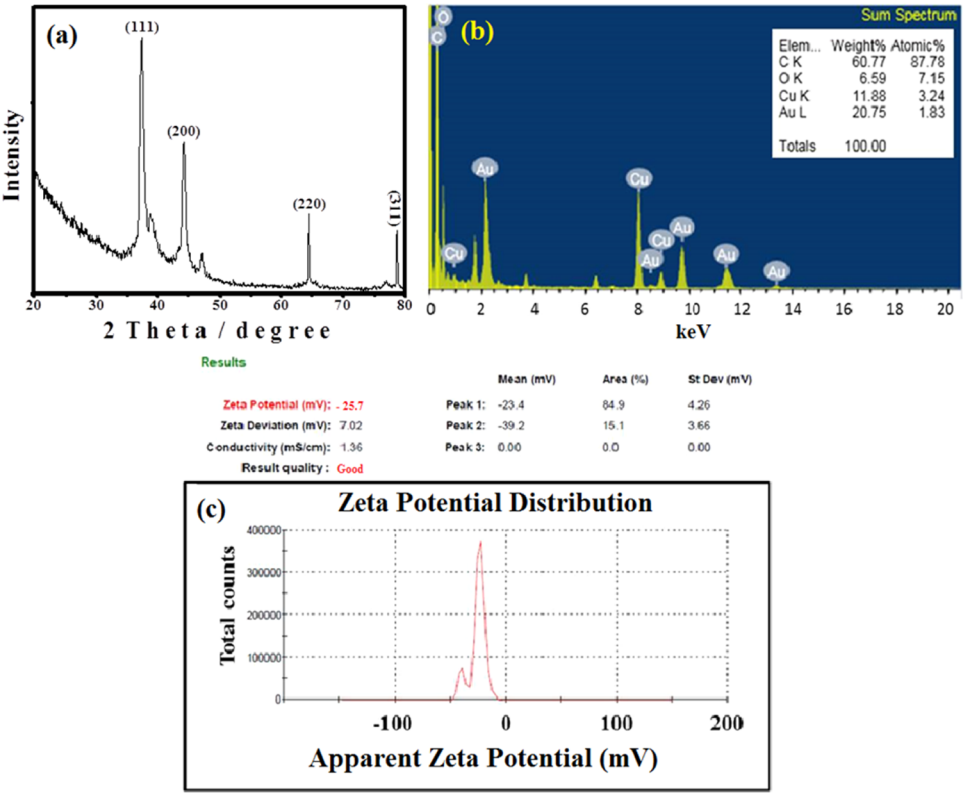

Figure 5. (a) XRD spectrum of *Zi*-AuNPs. (b) Energy-dispersive X-ray (EDX) spectrum of *Zi*-AuNPs: inset: elemental analysis. (c) ζ-Potential of *Zi*-AuNPs.

ppm since the pH is postulated to be the most influential factor on the photodegradation process because the variation in pH usually influences the surface charge, adsorption ability, and electron transfer capability of the photocatalyst, consequently affecting the photodegradation rate.[38] When the photodegradation process was carried out under highly acidic conditions (pH 2), the removal efficiency was about 56.5%. Afterward, the removal efficiency increased to 60.5 and 81.14% with increasing the pH value to 4 and 6. However, the degradation efficiency diminished to approximately 76% when

https://doi.org/10.1021/acsomega.1c06714
ACS Omega 2022, 7, 3121−3133

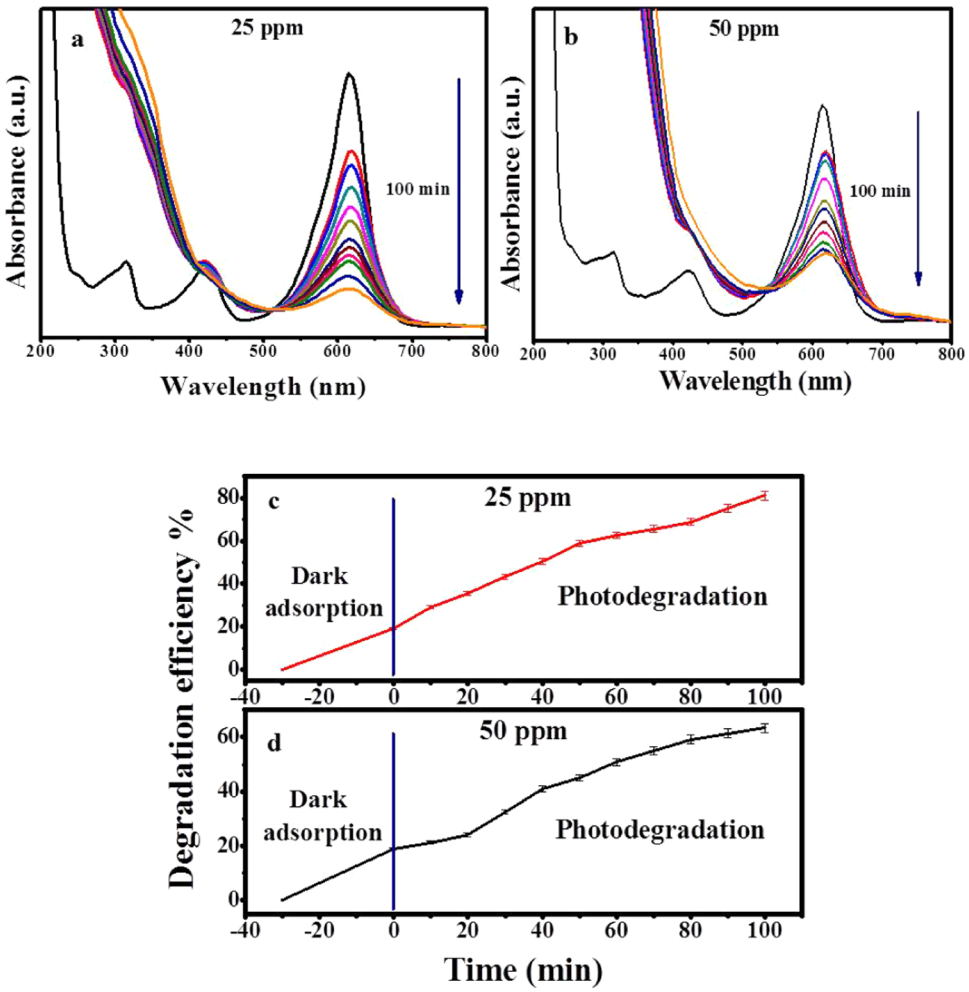

Figure 6. UV−visible absorption spectra of photodegradation of MG by *Zi*-AuNPs using different MG concentrations: (a) 25 ppm and (b) 50 ppm. Effect of time on the photodegradation of MG at concentrations of (c) 25 ppm and (d) 50 ppm.

the pH value was 8, denoting that the optimum pH level is 6. Thus, it was concluded that *Zi*-AuNPs could be applied as a photocatalyst for the photodegradation of MG over various pH levels as shown in Figure 7a.

Concerning the influence of temperature on MG removal with the concentration of 25 ppm in 100 min and under the optimum pH that is 6 (Figure 7b), the removal efficiency was recorded to be 67.85% when the temperature was 10 °C. Yet, the efficiency increased to approximately 81 and 84.7% when the temperature was set at 25 and 40 °C, respectively. Therefore, it was determined that by increasing temperature, the photodegradation process becomes enhanced due to the excessive release of hydroxyl radicals, which is in agreement with other previously published works.[39] However, the average temperature (25 °C) was used for the rest of the experimental work to simulate the natural conditions, which are usually found in wastewater.

To determine the effect of free radicals such as H_2O_2 on the photodegradation of MG, four different concentrations of H_2O_2 (25, 50, 75, and 100 mM) were applied to the MG solutions (25 ppm) with a pH of 6 for 100 min as presented in Figure 7c. The obtained photodegradation percentage was approximately 87.22% when the radical concentration was 25 mM. Then, on increasing the concentration of H_2O_2 to 50, 75, and 100 mM, the removal efficiency was enhanced to 87.88, 90.38, and 91.42%, respectively. Therefore, the positive effect of H_2O_2 addition was proven through the improvement of MG removal by increasing the concentration of H_2O_2 that could be accredited to the release of hydroxyl groups that led to the provision of more hydroxyl radicals to the photodegradation system.[40]

When the stability and recycling of *Zi*-AuNPs as a photocatalyst was investigated (Figure 7d) within 100 min of photocatalytic degradation of 25 ppm MG under pH 6, it was observed that the efficiency diminished from 81 to 69.2% after five recycling times, signifying the high applicability of *Zi*-AuNPs regeneration. The kinetics study of MG removal with the concentration of 25 ppm by *Zi*-AuNPs is presented in Figure 7e, in which the rate constant (K) was found to be 0.0129 min^{-1}. The obtained K in this study was suggested to be better than other previously reported studies on the photodegradation of MG, such as Tsvetkov et al.,[41] who reported rate constants of 0.0083 and 0.0073 min^{-1} for MgFO/AgNPs and $ZnFe_2O_4$ nanocomposites, respectively, as well as better than Sharma et al.[42] who reported a rate constant of 0.0102 min^{-1} using a nanocomposite hydrogel.

According to the above-mentioned results, it was determined that *Zi*-AuNPs is a promising photocatalyst that could proficiently be employed in wastewater treatment *via* the degradation of toxic organic pollutants. Furthermore, the effect of time on the photodegradation process of the two concentrations of MG is presented in Figure 6c,d. A

https://doi.org/10.1021/acsomega.1c06714
ACS Omega 2022, 7, 3121−3133

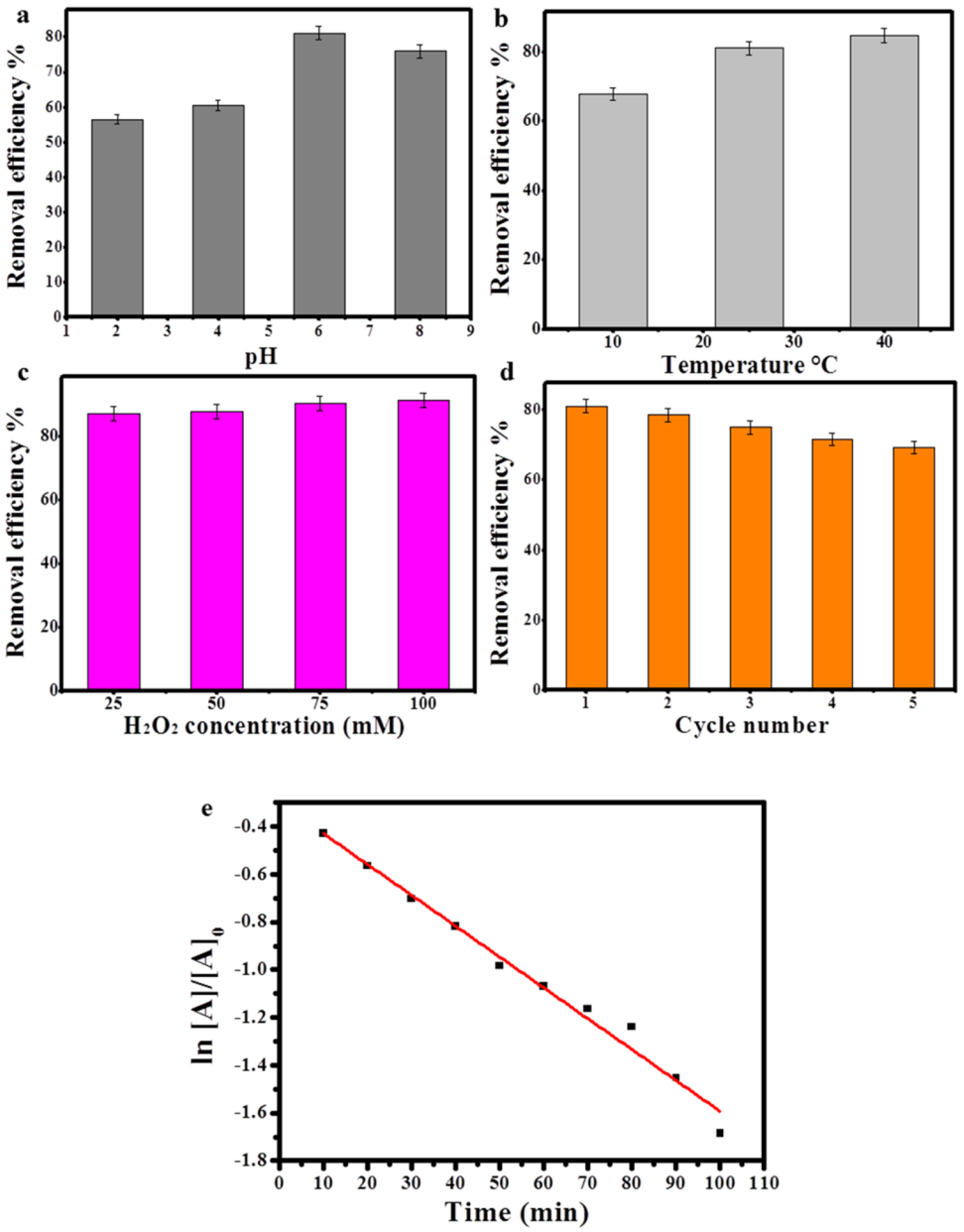

Figure 7. Effect of (a) pH, (b) temperature, and (c) H_2O_2 concentration on the removal efficiency of MG. (d) Recycling of *Zi*-AuNPs in MG removal. (e) Kinetics of MG removal by *Zi*-AuNPs.

comparison of the photodegradation efficacies between *Zi*-AuNPs and other photocatalysts utilized in MG photodegradation is presented in Table 1.

A mechanism for the photodegradation of MG is demonstrated in Figure 8, in which *Zi*-AuNPs resulted in MG degradation into simple, nontoxic, and inorganic products such as CO_2 and H_2O. The photodegradation process of MG is simply demonstrated through charge transfer procedures, which were previously elaborated in refs 43 and 44 through the following equations

$$MG^* + AuNPs \rightarrow MG^{*+} + AuNPs(e^-) \quad (1)$$

$$AuNPs(e^-) + O_2 \rightarrow O_2^* \quad (2)$$

$$O_2^* + H_2O \rightarrow H_2O_2 \rightarrow OH^* \quad (3)$$

$$O_2^* \text{ or } OH^* + MG \rightarrow CO_2 + H_2O + \text{byproducts} \quad (4)$$

By absorbing UV light, MG adsorbed on the surface of *Zi*-AuNPs became excited and commenced to donate its electrons to the conduction band of *Zi*-AuNPs. Afterward, these electrons were scavenged by dissolved oxygen and resulted in the formation of a highly reactive superoxide oxygen radical (O_2^*). Moreover, the O_2^* can react with H_2O adsorbed on the MG surface to form H_2O_2 that is promptly transformed into OH*. Eventually, both O_2^* and OH* led to the degradation of MG into CO_2, H_2O, and byproducts. The obtained results are similar to Huang et al.[45] and Li et al.[46] who clarified the important role of reactive oxygen species (ROS) in the photocatalytic degradation of different organic pollutants.

2.8. Estimation of Cell Viability—3-(4,5-Dimethylthiazol-2-yl)-2,5-diphenyltetrazolium Bromide (MTT) Assay. A variety of unique properties of AuNPs enabled them to be utilized as drug delivery carriers. These properties include small particle size, nontoxicity, and low levels of

https://doi.org/10.1021/acsomega.1c06714
ACS Omega 2022, 7, 3121−3133

Table 1. Comparison of Photodegradation Efficacies between *Zi*-AuNPs and Other Photocatalysts against MG

catalyst	dye concentration (ppm)	degradation efficiency (%)	time (min)	ref
$CuFe_2O_4$	18	62.37	210	47
ZnO	5	49	60	48
ZnO modified with EDTA		94.14		
$CdSe/TiO_2$	10	99	360	49
chitosan-supported ZnO	5	~100	90	50
Pd/WO_3 photocatalyst	5	66.66	360	51
Au−ZnO nanofilm	10	76.92	240	52
Zi-AuNPs	25	81.14	100	current study
	50	63.29		

immunogenicity.[53] Therefore, they were extensively utilized in cancer treatment. As tumor-targeting delivery materials get smaller like AuNPs, the possibility of them bypassing the body's natural barriers becomes better.[54]

Apoptosis is inhibited by physiological ATP levels, so ATP is thought to control apoptotic signals.[55] Caspase is supposed to play a crucial role in programmed cell death in a group of protease enzymes, and its activation is believed to depend on intracellular ATP concentrations,[56] so a drop in the ATP level after the addition of *Zi*-AuNPs might be presumed accountable for causing apoptosis via caspase pathways and resulting in cell death. Green synthesized AuNPs were also proved to be responsible for the release of ROS in a dose-dependent manner.[57] ROS are generally toxic to cancer cells, and their role in the cellular death process is deemed to be indispensable.[58] Additionally, affecting cell membrane integrity, disrupting ATP synthesis, and obstructing electron transfer are deemed to be the most commonly induced disorders when *Zi*-AuNPs interacted with MCF7 cancer cells that led to cell shrinkage and apoptosis.[59]

In this study, the anticancer efficacies of *Zi*-AuNPs and *Z. spina-christi* extract were examined against MCF7 utilizing MTT assay. The acquired results indicated that both samples exhibited good anticancer performance as the recorded cell viabilities were 35.73 and 25.44% at the highest concentration (100 μg/mL) of *Zi*-AuNPs (Figure 9a) and *Z. spina-christi* extract (Figure 9b), respectively. This may possibly be accredited to their capability of penetrating cell membrane, interacting with and disrupting proteins and other biomolecules.

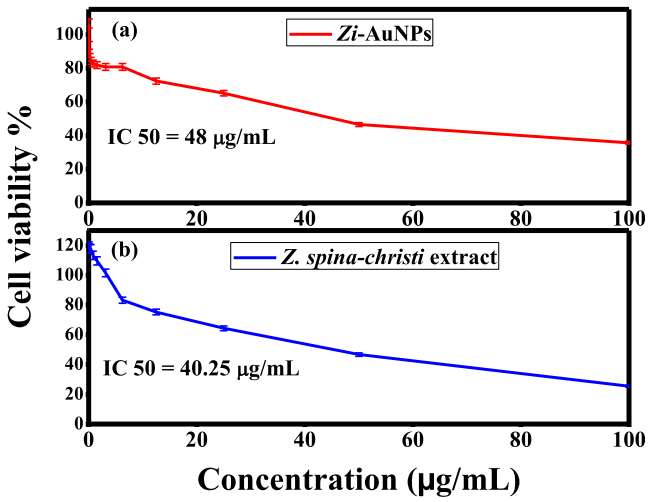

Figure 9. Anticancer efficiency % of (a) *Zi*-AuNPs and (b) *Z. spina-christi* extract against MCF7 cancer cells.

Zi-AuNPs and *Z. spina-christi* extract acquired IC_{50} concentrations of 48 and 40.25 μg/mL, respectively, signifying good efficacy in cancer treatment. A comparison between *Zi*-AuNPs and other synthesized AuNPs to indicate the higher cytotoxic efficiency of *Zi*-AuNPs is presented in Table 2.

2.9. Antioxidant Test. Antioxidants, such as metallic nanoparticles, play a significant role in the fight against free radicals like DPPH which is a commonly harmful free radical.[65] Regarding the mechanism of the DPPH assay, it was concluded that *via* receiving a hydrogen atom or an electron from an antioxidant such as *Zi*-AuNPs, the OH-DPPH solution was altered into the nonradical form of DPPH-H, thus leading

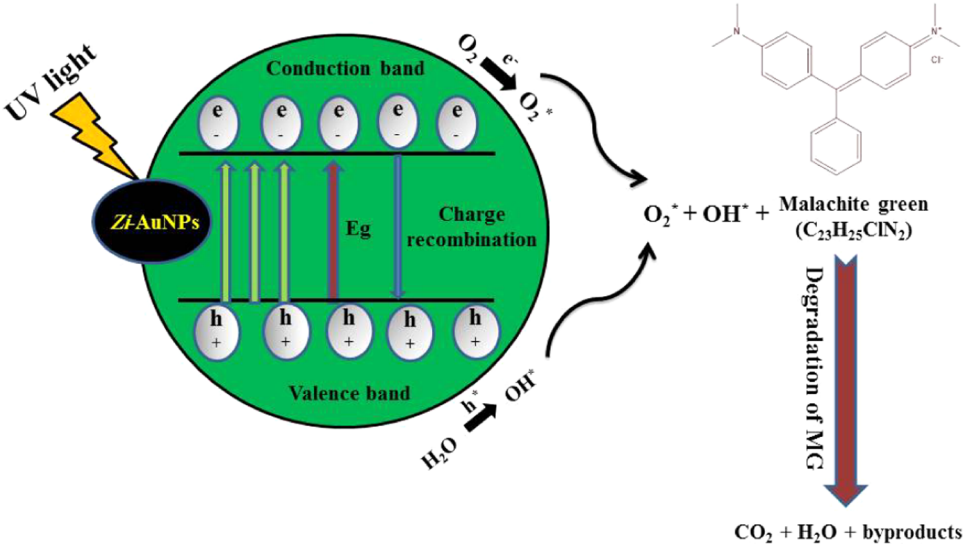

Figure 8. Probable mechanism of the photodegradation of MG by *Zi*-AuNPs.

https://doi.org/10.1021/acsomega.1c06714
ACS Omega 2022, 7, 3121−3133

Table 2. Comparison of Cytotoxic Efficiencies between *Zi*-AuNPs and Other Gold Nanoparticles

anticancer agent	concentration (μg/mL)	cell viability (%)	ref
AuNPs	250	40	60
AuNPs	320	10	61
AuNPs	10	40	62
AuNPs	120	45	63
AuNPs	100	38.7	64
Zi-AuNPs	100	35.73	current study

to DPPH removal. The assay was intended to detect the difference in DPPH concentration resulted from the reaction of DPPH with *Zi*-AuNPs using a spectrophotometer. Accordingly, the reception of an electron given by *Zi*-AuNPs led to the degradation of DPPH, which was determined quantitatively *via* the absorbance changes at 517 nm.

Using *Zi*-AuNPs to prevent the oxidative chain reaction from starting results in the generation of nonreactive radicals, which is what the antioxidant activity concept refers to. It was also found that AuNPs, particularly those made using biological or green methods, have significant antioxidant potential to control oxidative damage.[28] Another important point to keep in mind is that *Zi*-AuNPs' antioxidant activity is reliant on the phytoconstituents that are capping the nanoparticles.

In the current work, Figure 10 indicates that all of the samples had an inhibitory effect against DPPH in a concentration-dependent manner. Both *Z. spina-christi* extract and *Zi*-AuNPs demonstrated high efficacies of DPPH removal of about 92.34 and 67.5%, respectively, at a concentration of 100 μg/mL. The scavenging activity of vitamin C that was used as a reference was found to be less efficient since it removed about 55.84% of DPPH at the same concentration. It should be noted that the presence of numerous phytoconstituents such as flavonoids on the surface of *Zi*-AuNPs could be liable for their boosted antioxidant efficacy as previously deduced.[59]

Other workers have concluded that plants with high reducing ability also have a high antioxidant efficiency.[66,67] The antioxidant potency of *Z. spina-christi* is well reported.[24] As a result, the aqueous extract of *Z. spina-christi* was found to be a better antioxidant, as evidenced by the rapid transformation of Au^{3+} into *Zi*-AuNPs after the addition of the extract.

Similarly to the obtained results, other workers reported higher antioxidant efficacies of aqueous plant extracts than AuNPs fabricated *via* these extracts, such as Zayed et al.,[68] who mentioned that *Pimpinella anisum* extract was a more efficient antioxidant compared to AuNPs, and Sathishkumar et al.,[69] who indicated a higher inhibitory efficacy for *Couroupita guianensis* extract compared to phytosynthesized AuNPs. Additionally, Nakkala et al.[70] reported a higher antioxidant efficiency for *Costus pictus* extract than AuNPs phytoproduced by the same extract. A comparison among *Zi*-AuNPs and other metallic nanoparticles in the scavenging efficiency of DPPH is presented in Table 3.

Table 3. Comparison of Antioxidant Efficiencies between *Zi*-AuNPs and Other Metal Nanoparticles

antioxidant	concentration (μg/mL)	scavenging activity	ref
PtNPs	100	70	71
PtNPs		30	72
AgNPs	4	80	73
AgNPs	250	85.9	74
AuNPs	300	57.70	59
Zi-AuNPs	100	67.5	current study

3. CONCLUSIONS

According to the aforementioned results, the following conclusions could be drawn. *Z. spina-christi* extract played a dual role of a reducing agent and a stabilizing agent in a single-step process for the synthesis of *Zi*-AuNPs that remained stable for almost 3 months. FT-IR results revealed that the phytoconstituents of *Z. spina-christi* extract such as flavonoids, glycosides, terpenoids, and tannins were accountable for reducing and preserving the stability of the phytosynthesized AuNPs, which were majorly spherical with a surface plasmon

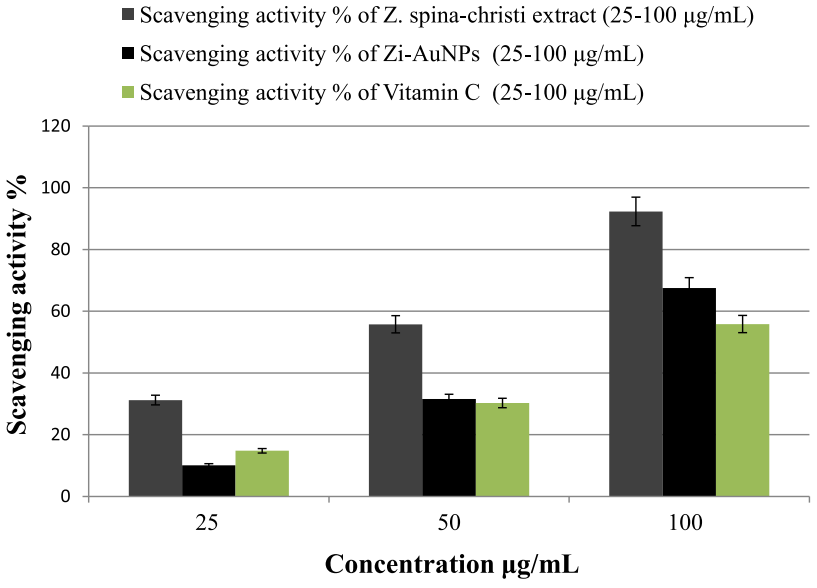

Figure 10. DPPH scavenging activity % of *Z. spina-christi* extract, *Zi*-AuNPs, and vitamin C (reference).

https://doi.org/10.1021/acsomega.1c06714
ACS Omega 2022, 7, 3121−3133

peak at 540 nm and a surface charge of −25.7 mV. Moreover, rod, triangle, rhomboid, pentagonal, and other irregular shapes were also detected. Crystalline nature with an FCC structure and a small particle size range of 0−10 nm were also confirmed. Furthermore, the crystallite size was measured and found to be 4.18 nm. Photodegradation results indicated the good applicability of *Zi*-AuNPs as a photocatalyst against MG with a photodegradation efficiency of 81.14% and good recycling capacity that was 69.2% after five cycles of regeneration. The high efficiencies of both *Zi*-AuNPs and *Z. spina-christi* extract as efficient anticancer agents against MCF7 cancer cells with cell viabilities of 35.73 and 25.44% for *Zi*-AuNPs and *Z. spina-christi*, respectively, were confirmed. Prominent antioxidant efficiencies were proven with DPPH scavenging percentages of 67.5% for *Zi*-AuNPs and 92.34% for *Z. spina-christi* extract.

4. MATERIALS AND METHODS

4.1. Chemicals and Reagents. All of the reagents employed in the current work were of high purity, including gold tetrachloroaurate solution ($HAuCl_4{\cdot}3H_2O$), 2,2-diphenyl-1-picrylhydrazyl (DPPH) (99%), ascorbic acid, and methylene blue (MB), that were purchased from Merck. Dimethyl sulfoxide (DMSO) was purchased from HiMedia (India), and the MCF7 cancer cell line was purchased from Vacsera center, Giza, Egypt.

4.2. Preparation of Plant Extract. To remove impurities and undesired elements, *Z. spina-christi* leaves were repeatedly rinsed with deionized water (DW). After that, it was fractured and let to dry in the open air before being dried in the oven overnight at 60 °C. After that, dry leaves were pulverized into a fine powder in a stainless steel mixer. The resulting powder (5 g) was mixed in 100 mL of DW, and then the mixture was agitated and heated for about 20 min until it was boiling.[22] Finally, the heated solution was filtered, and the filtrate extract was kept at a temperature of 4.0 °C for further use.[59]

4.3. Biosynthesis of *Zi*-AuNPs. In brief, 10 mL of the leaves extract was mixed with 1 mL of $HAuCl_4{\cdot}3H_2O$ (0.011 M). As a result, after 5 min of heating and stirring, the color changed from light brown to brownish-black. The purification phase involved centrifuging the *Zi*-AuNPs colloidal solution, collecting the precipitated pellets, and washing them with DW. To purify AuNPs once they were generated, this step was done three times. The colloidal solution was then kept at 4.0 °C for later use.[59]

4.4. Characterization Techniques. The size and shape of AuNPs were determined by HRTEM measurements performed on a JOEL, JEM-2100F, Japan, with an accelerating voltage of 200 kV. The formation of AuNPs was monitored by the UV−vis spectroscopy measurements on a double-beam T70/T80 series UV/vis spectrophotometer (PG Instruments Ltd., U.K.).[36] Furthermore, the FT-IR spectrum measurements were conducted for the ground sample with KBr on a JASCO spectrometer over the range 4000−600 cm^{-1}. The ζ-potential of AuNPs was determined by a ζ-potential analyzer (Zetasizer Nano ZS Malvern). XRD measurements of powdered AuNPs were conducted on an X-ray diffractometer (X'Pert PRO, the Netherlands) operated at a voltage of 45 kV and current of 40 mA with Cu $K\alpha_1$ radiation (λ = 1.54056 Å) in the 2θ range of 20−80°. The crystallite size was calculated from the width of the XRD peaks using the Scherrer formula[59] given by

$$(D) = \frac{0.9\lambda}{\beta \cos\theta}$$

where D is the average crystallite size, β indicates the line broadening the value of the full width at half-maximum (FWHM) of a peak, λ is the wavelength of irradiated X-rays, and θ is the maximum peak position value. Elements were determined by energy-dispersive X-ray (EDX) spectroscopy, JEOL model JSM-IT100.

4.5. Photocatalytic Experiments. The photocatalytic activity of the green synthesized *Zi*-AuNPs against MG dye was evaluated. *Zi*-AuNPs (10 mg) was added to 10 mL of two different concentrations of MG solution (25 and 50 ppm). Various levels of pH were examined, including 2, 4, 6, and 8. Three different temperatures were tested comprising 10, 25, and 40 °C. Furthermore, the effect of free radicals such as H_2O_2 was inspected using four different concentrations (25, 50, 75, and 100 mM). All of these factors were optimized to achieve the best photocatalytic removal of MG. Test solutions were mixed for 30 min in the dark for adsorption/desorption equilibration.[75] Subsequently, the solutions were stirred under a xenon lamp as a UV light source (λ > 400 nm) and monitored.[76] Next, 2 mL aliquots were removed and centrifuged at 17 000 rpm for 1 min to separate the solid nanocatalyst.[77] The absorbance of the resultant supernatant of MG solutions was measured at a 610 nm wavelength using UV−vis spectroscopy (T70/T80 series UV/vis spectrophotometer, PG Instruments Ltd., U.K.).[36] The percentage of MG degradation was calculated by the following formula

$$\%\ \text{degradation} = \frac{A_o}{A} \times 100 \tag{5}$$

where A_0 represents the initial absorbance and A refers to the final absorbance.

Regarding the recycling process, *Zi*-AuNPs were first removed from the solution by centrifugation at 17 000 rpm for 1 min, then thoroughly washed with DW, and eventually dried overnight in the oven.

4.6. Estimation of Cell Viability—MTT Assay. The effect of AuNPs on MCF7 cells was assessed by 3-(4,5-dimethylthiazol-2-yl)-2,5-diphenyltetrazolium bromide (MTT) assay.[32] Briefly, the cells (2×10^5 cells) were treated with various concentrations of *Zi*-AuNPs and *Z. spina-christi* extract (0.097−100 μg/mL) separately and incubated at 37 °C for 48 h using a CO_2 incubator. Over the incubation period, 10 μL of MTT solution (5 mg/mL) was added and the cells were incubated again for 4 h. The formed purple color formazone crystals were dissolved in 100 μL of dimethyl sulfoxide (DMSO), and the intensity was measured at 570 nm. The experiment was conducted in triplicate, and the percentage of cell viability was calculated by eq 2

$$\text{percentage of viability} = \frac{(\text{OD value of experimental sample})}{(\text{OD value of experimental control})} \times 100 \tag{6}$$

where OD stands for the optical density that was measured at average room temperature 25 °C and atmospheric pressure 1 atm.

4.7. Antioxidant Activity of AuNPs (DPPH Assay). The free radical scavenging activity was examined via DPPH assay to determine the antioxidant efficiency of *Zi*-AuNPs and *Z. spina-christi* extract. The assay was conducted in triplicate. In

https://doi.org/10.1021/acsomega.1c06714
ACS Omega 2022, 7, 3121−3133

the process, 1 mL of *Zi*-AuNPs and *Z. spina-christi* extract was mixed separately with 1 mL of DPPH (0.2 mM) along with control DPPH that does not contain any nanoparticles. The two mixtures were blended for 3 min in the dark at ambient temperature. Then, after 20 min, the concentration of radical is examined by the reduction in absorbance percentage of the mixture at 517 nm wavelength. Vitamin C (ascorbic acid) was used as a reference. The radical scavenging activity was determined by the following equation

$$\text{radical scavenging activity} = \frac{(\text{control absorbance} - \text{sample absorbance}) \times 100}{\text{control absorbance}} \quad (7)$$

where control absorbance is the absorbance in the absence of antioxidants and sample absorbance is the absorbance in the presence of antioxidants (*Zi*-AuNPs, *Z. spina-christi* extract, and vitamin C) at 517 nm.

4.8. Statistical Analysis. All experiments were conducted in triplicate ($n = 3$), while the gained data were presented as a mean value corrected by the standard deviation (±SD).

AUTHOR INFORMATION

Corresponding Authors

Mohamed Hosny − *Green Technology Group, Environmental Sciences Department, Faculty of Science, Alexandria University, Alexandria 21511, Egypt;* orcid.org/0000-0001-6824-5459; Email: MohamedHosny@alexu.edu.eg, mohamedhosnymetal09@gmail.com

Abdelazeem S. Eltaweil − *Department of Chemistry, Faculty of Science, Alexandria University, Alexandria 21321, Egypt;* orcid.org/0000-0001-8912-1244; Email: abdelazeemeltaweil@alexu.edu.eg

Authors

Mohamed Mostafa − *Department of Botany and Microbiology, Faculty of Science, Alexandria University, Alexandria 21321, Egypt*

Yaser A. El-Badry − *Chemistry Department, Faculty of Science, Taif University, Taif 21944, Saudi Arabia*

Enas E. Hussein − *National Water Research Center, Shubra El-Kheima 13411, Egypt*

Ahmed M. Omer − *Polymer Materials Research Department, Advanced Technology and New Materials Research Institute, City of Scientific Research and Technological Applications (SRTA-City), New Borg El-Arab City 21934 Alexandria, Egypt*

Manal Fawzy − *Green Technology Group, Environmental Sciences Department, Faculty of Science, Alexandria University, Alexandria 21511, Egypt; National Egyptian Biotechnology Experts Network, National Egyptian Academy for Scientific Research and Technology, Cairo 33516 Cairo Governorate, Egypt;* orcid.org/0000-0002-9401-9049

Complete contact information is available at: https://pubs.acs.org/10.1021/acsomega.1c06714

Author Contributions

M.H. carried out the experimental work, data analysis, and writing the original draft. A.S.E. was responsible for the investigation, methodology, visualization, and supervision. M.M. was responsible for conducting the experimental work and data curation. Y.A.E.-B. was responsible for visualization and supervision. E.E.H. was responsible for data analysis and data curation. A.M.O. was responsible for supervision. M.F. was responsible for conceptualization, supervision, validation, and reviewing the final manuscript.

Notes

The authors declare no competing financial interest.

ACKNOWLEDGMENTS

The authors would like to acknowledge the financial support provided from Taif University Researchers Supporting Project Number (TURSP-2020/106) Taif University, Taif, Saudi Arabia.

REFERENCES

(1) Jadoun, S.; Arif, R.; Jangid, N. K.; Meena, R. K. Green synthesis of nanoparticles using plant extracts: A review. *Environ. Chem. Lett.* **2021**, *19*, 355−374.

(2) Liu, S.; Tian, J.; Wang, L.; Luo, Y.; Sun, X. One-pot synthesis of CuO nanoflower-decorated reduced graphene oxide and its application to photocatalytic degradation of dyes. *Catal. Sci. Technol.* **2012**, *2*, 339−344.

(3) Hosny, M.; Fawzy, M.; El-Fakharany, E. M.; Omer, A. M.; El-Monaem, E. M. A.; Khalifa, R. E.; Eltaweil, A. S. Biogenic synthesis, characterization, antimicrobial, antioxidant, antidiabetic, and catalytic applications of platinum nanoparticles synthesized from *Polygonum salicifolium* leaves. *J. Environ. Chem. Eng.* **2022**, *10*, No. 106806.

(4) Attia, N. F.; Park, J.; Oh, H. Facile tool for green synthesis of graphene sheets and their smart free-standing UV protective film. *Appl. Surf. Sci.* **2018**, *458*, 425−430.

(5) Asiya, S.; Pal, K.; Kralj, S.; El-Sayyad, G.; de Souza, F.; Narayanan, T. Sustainable preparation of gold nanoparticles via green chemistry approach for biogenic applications. *Mater. Today Chem.* **2020**, *17*, No. 100327.

(6) Attia, N. F.; Eid, A. M.; Soliman, M. A.; Nagy, M. Exfoliation and decoration of graphene sheets with silver nanoparticles and their antibacterial properties. *J. Polym. Environ.* **2018**, *26*, 1072−1077.

(7) Hameed, S.; Ali Shah, S.; Iqbal, J.; Numan, M.; Muhammad, W.; Junaid, M.; Shah, S.; Khurshid, R.; Umer, F. *Cannabis sativa*-mediated synthesis of gold nanoparticles and their biomedical properties. *Bioinspired, Biomimetic Nanobiomater.* **2020**, *9*, 95−102.

(8) Guo, Y.; Jiang, N.; Zhang, L.; Yin, M. Green synthesis of gold nanoparticles from Fritillaria cirrhosa and its anti-diabetic activity on Streptozotocin induced rats. *Arab. J. Chem.* **2020**, *13*, 5096−5106.

(9) El-Borady, O. M.; Fawzy, M.; Hosny, M. Antioxidant, anticancer and enhanced photocatalytic potentials of gold nanoparticles biosynthesized by common reed leaf extract. *Appl. Nanosci.* **2021**, 1−12.

(10) Abdelfatah, A. M.; Fawzy, M.; Eltaweil, A. S.; El-Khouly, M. E. Green Synthesis of Nano-Zero-Valent Iron Using *Ricinus communis* Seeds Extract: Characterization and Application in the Treatment of Methylene Blue-Polluted Water. *ACS Omega* **2021**, 25397.

(11) Elahi, N.; Kamali, M.; Baghersad, M. H. Recent biomedical applications of gold nanoparticles: A review. *Talanta* **2018**, *184*, 537−556.

(12) El-Maghrabi, N.; El-Borady, O. M.; Hosny, M.; Fawzy, M. Catalytic and Medical Potential of a Phyto-Functionalized Reduced Graphene Oxide−Gold Nanocomposite Using Willow-Leaved Knot-grass. *ACS Omega* **2021**, 34954.

(13) Rajeshkumar, S.; Malarkodi, C.; Al Farraj, D. A.; Elshikh, M. S.; Roopan, S. M. Employing sulphated polysaccharide (fucoidan) as medium for gold nanoparticles preparation and its anticancer study against HepG2 cell lines. *Mater. Today Commun.* **2021**, *26*, No. 101975.

(14) Sadegh, H.; Ali, G. A.; Gupta, V. K.; Makhlouf, A. S. H.; Shahryari-Ghoshekandi, R.; Nadagouda, M. N.; Sillanpää, M.; Megiel, E. The role of nanomaterials as effective adsorbents and their

applications in wastewater treatment. *J. Nanostruct. Chem.* **2017**, *7*, 1−14.
(15) Cheng, N.; Tian, J.; Liu, Q.; Ge, C.; Qusti, A. H.; Asiri, A. M.; Al-Youbi, A. O.; Sun, X. Au-nanoparticle-loaded graphitic carbon nitride nanosheets: green photocatalytic synthesis and application toward the degradation of organic pollutants. *ACS Appl. Mater. Interfaces* **2013**, *5*, 6815−6819.
(16) Jiang, Y.; Zhao, H.; Liang, J.; Yue, L.; Li, T.; Luo, Y.; Liu, Q.; Lu, S.; Asiri, A. M.; Gong, Z.; Sun, X. Anodic oxidation for the degradation of organic pollutants: anode materials, operating conditions and mechanisms. A mini review. *Electrochem. Commun.* **2021**, No. 106912.
(17) Srivastava, S.; Sinha, R.; Roy, D. Toxicological effects of malachite green. *Aquat. Toxicol.* **2004**, *66*, 319−329.
(18) Shunmugam, R.; Balusamy, S. R.; Kumar, V.; Menon, S.; Lakshmi, T.; Perumalsamy, H. Biosynthesis of gold nanoparticles using marine microbe (*Vibrio alginolyticus*) and its anticancer and antioxidant analysis. *J. King Saud Univ., Sci.* **2021**, *33*, No. 101260.
(19) Rajeshkumar, S. Anticancer activity of eco-friendly gold nanoparticles against lung and liver cancer cells. *J. Genet. Eng. Biotechnol.* **2016**, *14*, 195−202.
(20) Xia, Y.; You, P.; Xu, F.; Liu, J.; Xing, F. Novel functionalized selenium nanoparticles for enhanced anti-hepatocarcinoma activity in vitro. *Nanoscale Res. Lett.* **2015**, *10*, No. 349.
(21) Pu, S.; Li, J.; Sun, L.; Zhong, L.; Ma, Q. An in vitro comparison of the antioxidant activities of chitosan and green synthesized gold nanoparticles. *Carbohydr. Polym.* **2019**, *211*, 161−172.
(22) Eltaweil, A. S.; Fawzy, M.; Hosny, M.; Abd El-Monaem, E. M.; Tamer, T. M.; Omer, A. M. Green synthesis of platinum nanoparticles using *Atriplex halimus* leaves for potential antimicrobial, antioxidant, and catalytic applications. *Arab. J. Chem.* **2021**, No. 103517.
(23) Yossef, H.; Khedr, A. A.; Mahran, M. Z. Hepatoprotective activity and antioxidant effects of El Nabka (*Zizyphus spina-christi*) fruits on rats hepatotoxicity induced by carbon tetrachloride. *Nat. Sci.* **2011**, *9*, 1−7.
(24) Asgarpanah, J.; Haghighat, E. Phytochemistry and pharmacologic properties of *Ziziphus spina christi* (L.) Willd. *Afr. J. Pharm. Pharmacol.* **2012**, *6*, 2332−2339.
(25) Aly, S. A.; El-Rigal, N. S.; Rizk, M. Z. Nutritional Supplementation with *Ailanthus altissima* and *Ziziphus spina christi* to Compensate for Some Metabolic. *Pak. J. Biol. Sci.* **2006**, *9*, 1700−1706.
(26) Glombitza, K.-W.; Mahran, G.; Mirhom, Y.; Michel, K.; Motawi, T. Hypoglycemic and antihyperglycemic effects of *Zizyphus spina-christi* in rats. *Planta Med.* **1994**, *60*, 244−247.
(27) Sunderam, V.; Thiyagarajan, D.; Lawrence, A. V.; Mohammed, S. S. S.; Selvaraj, A. In-vitro antimicrobial and anticancer properties of green synthesized gold nanoparticles using *Anacardium occidentale* leaves extract. *Saudi J. Biol. Sci.* **2019**, *26*, 455−459.
(28) Chen, J.; Li, Y.; Fang, G.; Cao, Z.; Shang, Y.; Alfarraj, S.; Alharbi, S. A.; Li, J.; Yang, S.; Duan, X. Green synthesis, characterization, cytotoxicity, antioxidant, and anti-human ovarian cancer activities of *Curcumae kwangsiensis* leaf aqueous extract green-synthesized gold nanoparticles. *Arab. J. Chem.* **2021**, *14*, No. 103000.
(29) Rabeea, M. A.; Owaid, M. N.; Aziz, A. A.; Jameel, M. S.; Dheyab, M. A. Mycosynthesis of gold nanoparticles using the extract of *Flammulina velutipes*, Physalacriaceae, and their efficacy for decolorization of methylene blue. *J. Environ. Chem. Eng.* **2020**, *8*, No. 103841.
(30) Akintelu, S. A.; Yao, B.; Folorunso, A. S. Green synthesis, characterization, and antibacterial investigation of synthesized gold nanoparticles (AuNPs) from *Garcinia kola* pulp extract. *Plasmonics* **2021**, *16*, 157−165.
(31) Ebrahimzadeh, M. A.; Naghizadeh, A.; Mohammadi-Aghdam, S.; Khojasteh, H.; Ghoreishi, S. M.; Mortazavi-Derazkola, S. Enhanced catalytic and antibacterial efficiency of biosynthesized *Convolvulus fruticosus* extract capped gold nanoparticles (CFE@ AuNPs). *J. Photochem. Photobiol., B* **2020**, *209*, No. 111949.
(32) Manikandakrishnan, M.; Palanisamy, S.; Vinosha, M.; Kalanjiaraja, B.; Mohandoss, S.; Manikandan, R.; Tabarsa, M.; You, S.; Prabhu, N. M. Facile green route synthesis of gold nanoparticles using *Caulerpa racemosa* for biomedical applications. *J. Drug Delivery Sci. Technol.* **2019**, *54*, No. 101345.
(33) Omer, A. M.; El-Monaem, E. M. A.; El-Subruiti, G. M.; El-Latif, M. M.; Eltaweil, A. S. Fabrication of easy separable and reusable MIL-125 (Ti)/MIL-53 (Fe) binary MOF/CNT/Alginate composite microbeads for tetracycline removal from water bodies. *Sci. Rep.* **2021**, *11*, No. 23818.
(34) Eltaweil, A. S.; Mamdouh, I. M.; Abd El-Monaem, E. M.; El-Subruiti, G. M. Highly efficient removal for methylene blue and Cu2+ onto UiO-66 metal−organic framework/carboxylated graphene oxide-incorporated sodium alginate beads. *ACS Omega* **2021**, *6*, 23528−23541.
(35) Zhao, P.; El-kott, A.; Ahmed, A. E.; Khames, A.; Zein, M. A. Green synthesis of gold nanoparticles (Au NPs) using *Tribulus terrestris* extract: Investigation of its catalytic activity in the oxidation of sulfides to sulfoxides and study of its anti-acute leukemia activity. *Inorg. Chem. Commun.* **2021**, *131*, No. 108781.
(36) Hosny, M.; Fawzy, M.; Abdelfatah, A. M.; Fawzy, E. E.; Eltaweil, A. S. Comparative study on the potentialities of two halophytic species in the green synthesis of gold nanoparticles and their anticancer, antioxidant and catalytic efficiencies. *Adv. Powder Technol.* **2021**, DOI: 10.1016/j.apt.2021.07.008.
(37) Sathiyaraj, S.; Suriyakala, G.; Gandhi, A. D.; Babujanarthanam, R.; Almaary, K. S.; Chen, T.-W.; Kaviyarasu, K. Biosynthesis, characterization, and antibacterial activity of gold nanoparticles. *J. Infect. Public Health* **2021**, 1842.
(38) Kim, H.-J.; Phenrat, T.; Tilton, R. D.; Lowry, G. V. Effect of kaolinite, silica fines and pH on transport of polymer-modified zero valent iron nano-particles in heterogeneous porous media. *J. Colloid Interface Sci.* **2012**, *370*, 1−10.
(39) Huang, Y.; Lu, Y.; Lin, Y.; Mao, Y.; Ouyang, G.; Liu, H.; Zhang, S.; Tong, Y. Cerium-based hybrid nanorods for synergetic photo-thermocatalytic degradation of organic pollutants. *J. Mater. Chem. A* **2018**, *6*, 24740−24747.
(40) Liu, W.; Li, Z.; Kang, Q.; Wen, L. Efficient photocatalytic degradation of doxycycline by coupling α-Bi2O3/g-C3N4 composite and H2O2 under visible light. *Environ. Res.* **2021**, *197*, No. 110925.
(41) Tsvetkov, M.; Zaharieva, J.; Milanova, M. Ferrites, modified with silver nanoparticles, for photocatalytic degradation of malachite green in aqueous solutions. *Catal. Today* **2020**, *357*, 453−459.
(42) Sharma, G.; ALOthman, Z. A.; Kumar, A.; Sharma, S.; Ponnusamy, S. K.; Naushad, M. Fabrication and characterization of a nanocomposite hydrogel for combined photocatalytic degradation of a mixture of malachite green and fast green dye. *Nanotechnol. Environ. Eng.* **2017**, *2*, No. 4.
(43) Li, F.; Tao, R.; Cao, B.; Yang, L.; Wang, Z. Manipulating the Light-Matter Interaction of PtS/MoS2 p−n Junctions for High Performance Broadband Photodetection. *Adv. Funct. Mater.* **2021**, *31*, No. 2104367.
(44) Qin, T.; Wang, Z.; Wang, Y.; Besenbacher, F.; Otyepka, M.; Dong, M. Recent progress in emerging two-dimensional transition metal carbides. *Nanomicro Lett.* **2021**, *13*, No. 183.
(45) Huang, Y.; Xu, H.; Yang, H.; Lin, Y.; Liu, H.; Tong, Y. Efficient charges separation using advanced BiOI-based hollow spheres decorated with palladium and manganese dioxide nanoparticles. *ACS Sustainable Chem. Eng.* **2018**, *6*, 2751−2757.
(46) Li, Y.; Xia, Y.; Liu, K.; Ye, K.; Wang, Q.; Zhang, S.; Huang, Y.; Liu, H. Constructing Fe-MOF-derived Z-scheme photocatalysts with enhanced charge transport: nanointerface and carbon sheath synergistic effect. *ACS Appl. Mater. Interfaces* **2020**, *12*, 25494−25502.
(47) Yadav, P.; Surolia, P. K.; Vaya, D. Synthesis and application of copper ferrite-graphene oxide nanocomposite photocatalyst for the degradation of malachite green. *Mater. Today: Proc.* **2021**, *43*, 2949−2953.

https://doi.org/10.1021/acsomega.1c06714
ACS Omega 2022, 7, 3121−3133

(48) Meena, S.; Dipti, V.; Das, B. Photocatalytic degradation of Malachite Green dye by modified ZnO nanomaterial. *Bull. Mater. Sci.* **2016**, *39*, 1735−1743.
(49) Wang, P.; Li, D.; Chen, J.; Zhang, X.; Xian, J.; Yang, X.; Zheng, X.; Li, X.; Shao, Y. A novel and green method to synthesize CdSe quantum dots-modified TiO2 and its enhanced visible light photocatalytic activity. *Appl. Catal., B* **2014**, *160*−*161*, 217−226.
(50) Saad, A. M.; Abukhadra, M. R.; Ahmed, S. A.-K.; Elzanaty, A. M.; Mady, A. H.; Betiha, M. A.; Shim, J.-J.; Rabie, A. M. Photocatalytic degradation of malachite green dye using chitosan supported ZnO and Ce−ZnO nano-flowers under visible light. *J. Environ. Manage.* **2020**, *258*, No. 110043.
(51) Liu, Y.; Ohko, Y.; Zhang, R.; Yang, Y.; Zhang, Z. Degradation of malachite green on Pd/WO3 photocatalysts under simulated solar light. *J. Hazard. Mater.* **2010**, *184*, 386−391.
(52) Georgiev, P.; Kaneva, N.; Bojinova, A.; Papazova, K.; Mircheva, K.; Balashev, K. Effect of gold nanoparticles on the photocatalytic efficiency of ZnO films. *Colloids Surf., A* **2014**, *460*, 240−247.
(53) Parveen, A.; Rao, S. Cytotoxicity and genotoxicity of biosynthesized gold and silver nanoparticles on human cancer cell lines. *J. Clust. Sci.* **2015**, *26*, 775−788.
(54) Hosny, M.; Fawzy, M.; El-Borady, O. M.; Mahmoud, A. E. D. Comparative study between *Phragmites australis* root and rhizome extracts for mediating gold nanoparticles synthesis and their medical and environmental applications. *Adv. Powder Technol.* **2021**, *32*, 2268−2279.
(55) Garedew, A.; Henderson, S. O.; Moncada, S. Activated macrophages utilize glycolytic ATP to maintain mitochondrial membrane potential and prevent apoptotic cell death. *Cell Death Differ.* **2010**, *17*, 1540−1550.
(56) Song, Y.; Dong, Y.; Liao, Y.; Liang, Z.; Yao, J.; Zhou, X. Apoptotic caspases suppress *Mycobacterium bovis*-induced IFN-β production in murine macrophage. *J. Infect.* **2021**, 61.
(57) Pan, Y.; Neuss, S.; Leifert, A.; Fischler, M.; Wen, F.; Simon, U.; Schmid, G.; Brandau, W.; Jahnen-Dechent, W. Size-dependent cytotoxicity of gold nanoparticles. *Small* **2007**, *3*, 1941−1949.
(58) Li, T.; Li, F.; Xiang, W.; Yi, Y.; Chen, Y.; Cheng, L.; Liu, Z.; Xu, H. Selenium-containing amphiphiles reduced and stabilized gold nanoparticles: kill cancer cells via reactive oxygen species. *ACS Appl. Mater. Interfaces.* **2016**, *8*, 22106−22112.
(59) Hosny, M.; Fawzy, M. Instantaneous phytosynthesis of gold nanoparticles via Persicaria salicifolia leaf extract, and their medical applications. *Adv. Powder Technol.* **2021**, *32*, 2891−2904.
(60) Muthukumar, T.; Sudhakumari; Sambandam, B.; Aravinthan, A.; Sastry, T. P.; Kim, J.-H. Green synthesis of gold nanoparticles and their enhanced synergistic antitumor activity using HepG2 and MCF7 cells and its antibacterial effects. *Process Biochem.* **2016**, *51*, 384−391.
(61) Uzma, M.; Sunayana, N.; Raghavendra, V. B.; Madhu, C. S.; Shanmuganathan, R.; Brindhadevi, K. Biogenic synthesis of gold nanoparticles using *Commiphora wightii* and their cytotoxic effects on breast cancer cell line (MCF-7). *Process Biochem.* **2020**, *92*, 269−276.
(62) Uma Suganya, K. S.; Govindaraju, K.; Ganesh Kumar, V.; Prabhu, D.; Arulvasu, C.; Stalin Dhas, T.; Karthick, V.; Changmai, N. Anti-proliferative effect of biogenic gold nanoparticles against breast cancer cell lines (MDA-MB-231 & MCF-7). *Appl. Surf. Sci.* **2016**, *371*, 415−424.
(63) Vijayakumar, S. Eco-friendly synthesis of gold nanoparticles using fruit extracts and in vitro anticancer studies. *J. Saudi Chem. Soc.* **2019**, *23*, 753−761.
(64) Barai, A. C.; Paul, K.; Dey, A.; Manna, S.; Roy, S.; Bag, B. G.; Mukhopadhyay, C. Green synthesis of *Nerium oleander*-conjugated gold nanoparticles and study of its in vitro anticancer activity on MCF-7 cell lines and catalytic activity. *Nano Convergence* **2018**, *5*, No. 10.
(65) Bhakya, S.; Muthukrishnan, S.; Sukumaran, M.; Muthukumar, M. Biogenic synthesis of silver nanoparticles and their antioxidant and antibacterial activity. *Appl. Nanosci.* **2016**, *6*, 755−766.
(66) Karuppanapandian, T.; Moon, J.-C.; Kim, C.; Manoharan, K.; Kim, W. Reactive oxygen species in plants: their generation, signal transduction, and scavenging mechanisms. *Aust. J. Crop Sci.* **2011**, *5*, 709−725.
(67) Apel, K.; Hirt, H. Reactive oxygen species: metabolism, oxidative stress, and signal transduction. *Annu. Rev. Plant Biol.* **2004**, *55*, 373−399.
(68) Zayed, M. F.; Mahfoze, R. A.; El-kousy, S. M.; Al-Ashkar, E. A. In-vitro antioxidant and antimicrobial activities of metal nanoparticles biosynthesized using optimized *Pimpinella anisum* extract. *Colloids Surf., A* **2020**, *585*, No. 124167.
(69) Sathishkumar, G.; Jha, P. K.; Vignesh, V.; Rajkuberan, C.; Jeyaraj, M.; Selvakumar, M.; Jha, R.; Sivaramakrishnan, S. Cannonball fruit (*Couroupita guianensis*, Aubl.) extract mediated synthesis of gold nanoparticles and evaluation of its antioxidant activity. *J. Mol. Liq.* **2016**, *215*, 229−236.
(70) Nakkala, J. R.; Bhagat, E.; Suchiang, K.; Sadras, S. R. Comparative study of antioxidant and catalytic activity of silver and gold nanoparticles synthesized from *Costus pictus* leaf extract. *J. Mater. Sci. Technol.* **2015**, *31*, 986−994.
(71) Ramachandiran, D.; Elangovan, M.; Rajesh, K. Structural, optical, biological and photocatalytic activities of platinum nanoparticles using salixtetraspeama leaf extract via hydrothermal and ultrasonic methods. *Optik* **2021**, No. 167494.
(72) Ramkumar, V. S.; Pugazhendhi, A.; Prakash, S.; Ahila, N.; Vinoj, G.; Selvam, S.; Kumar, G.; Kannapiran, E.; Rajendran, R. B. Synthesis of platinum nanoparticles using seaweed *Padina gymnospora* and their catalytic activity as PVP/PtNPs nanocomposite towards biological applications. *Biomed. Pharmacother.* **2017**, *92*, 479−490.
(73) Sreelekha, E.; George, B.; Shyam, A.; Sajina, N.; Mathew, B. A comparative study on the synthesis, characterization, and antioxidant activity of green and chemically synthesized silver nanoparticles. *BioNanoScience* **2021**, *11*, 489−496.
(74) Kharat, S. N.; Mendhulkar, V. D. Synthesis, characterization and studies on antioxidant activity of silver nanoparticles using *Elephantopus scaber* leaf extract. *Mater. Sci. Eng., C* **2016**, *62*, 719−724.
(75) Bhati, A.; Anand, S. R.; Gunture; Garg, A. K.; Khare, P.; Sonkar, S. K. Sunlight-induced photocatalytic degradation of pollutant dye by highly fluorescent red-emitting Mg-N-embedded carbon dots. *ACS Sustainable Chem. Eng.* **2018**, *6*, 9246−9256.
(76) Paramanik, L.; Reddy, K. H.; Parida, K. Stupendous photocatalytic activity of p-BiOI/n-PbTiO3 heterojunction: the significant role of oxygen vacancies and interface coupling. *J. Phys. Chem. C* **2019**, *123*, 21593−21606.
(77) Zhang, J.; Wang, Y.; Jin, J.; Zhang, J.; Lin, Z.; Huang, F.; Yu, J. Efficient visible-light photocatalytic hydrogen evolution and enhanced photostability of core/shell CdS/g-C3N4 nanowires. *ACS Appl. Mater. Interfaces* **2013**, *5*, 10317−10324.

https://doi.org/10.1021/acsomega.1c06714
ACS Omega 2022, 7, 3121−3133